Eur. Phys. J. D **38**, 35–45 (2006)
DOI: 10.1140/epjd/e2006-00023-5

THE EUROPEAN PHYSICAL JOURNAL D

Fragmentation and internal steric rearrangement of C_{60}^- in electron transfer dynamics

R.F.M. Lobo[a], N.T. Silva, B.M.N. Vicente, I.M.V. Gouveia, F.M.V. Berardo, and J.H.F. Ribeiro

Grupo de Nanotecnologia e Ciência à Nano-Escala (GNCN), Faculdade de Ciências e Tecnologia, Universidade Nova de Lisboa, 2829-516 Caparica, Portugal

Received 19 July 2005 / Received in final form 10 October 2005
Published online 31 January 2006 –

Abstract. The crossed molecular beam technique is used for producing C_{60}^- species through potassium-buckyball collision processes, and studying the collision dynamics in an energy ranging from 10 eV up to 500 eV. At low collision energies only the negative parent ion is formed. As long as the collision energy is increased the fragmentation pattern of the fullerene negative ion could be identified and relative total cross-sections could be measured. Surprisingly, some satellite contributions have been observed in the band structure of C_{60}^- parent ion time-of-flight spectrum, which points to the existence of distinct conformational C_{60}^- isomers, which are likely to be formed during the collision, favoured by the strong polarization of the C_{60}^- in the presence of the K^+ projectile ion. Such presumed detection of different spheroidal metastable C_{60}^- conformers was made possible due to an electric effect operating at the nanoscale.

PACS. 34.50.Lf Chemical reactions, energy disposal, and angular distribution, as studied by atomic and molecular beams – 61.48.+c Fullerenes and fullerene-related materials – 71.20.Tx Fullerenes and related materials; intercalation compounds

1 Introduction

Molecular dissociation induced by electron attachment is a relevant process for many atmospherical, biological and industrial applications. In particular, fragmentation pathways of energy-rich molecular anions can be experimentally investigated, making use of electron transfer atom-molecule collisions [1–13]. In alkali atom-molecule collisions negative ionization of the molecular target is induced through electron transfer, where the alkali atom donates the electron to the molecule [1–8].

The number of scientific papers devoted to electron transfer in complex molecules has been increasing and here one focuses our particular attention on the fullerene C_{60}, one of the most significant clusters in the field of nanoscience and nanotechnology. This work includes original results of electron transfer in neutral atomic collisions with C_{60}, in a wide range of energies, well above the ion-pair formation threshold.

The collisional ionization process allows access to metastable states of the negative parent ion which are not attainable in simple electron attachment experiments, and leads in complex anions to negative fragmentation. Actually, it makes up a way of depositing energy in the form of vibrational excitation of the molecular parent ion, which is collisional energy dependent [10–12]. The vibronic excitation is mediated by a crossing of potentials of different electronic states, and the electronic transition transfers the system to another potential hypersurface that is a quite different function of the nuclear coordinates. In order to study the relation between electronic transition and vibrational motion, the most powerful instrumental tool is the molecular beam method [14]. The observation of molecular motion in the subpicosecond domain could be achieved with molecular beam techniques even before the modern femtosecond laser experiments. As the collision energy is in the eV region, one can probe the vibrational dynamics of the parent negative ion on a 10 fs timescale [8]. When the parent negative ion has a lifetime longer in comparison with fragmentation times, some energy can be distributed over the available internal degrees of freedom, and so influencing the fragment ionic yields produced.

Accordingly to the type of negative fragments detected by using several different molecular targets, it has been possible to distinguish two different kinds of negative fragmentation behaviors, which have been coined as *quasi-diatomic* and *non-diatomic* [12]. In the first case (observed in CH_3I, CH_3NO_2 and mono-halobenzenes among others [6–12]), the fragmentation of the polyatomic negative target is mostly dissociative with an intramolecular dynamics involving dominantly only one internal vibrational coordinate (in fact, in mono-halobenzenes only a minor fraction of ring fragmentation ions has been observed

[a] e-mail: rfl@fct.unl.pt

and the parent ion was not detected [12]). In the second case, the fragmentation occurs involving more than one internal coordinate, which usually leads to several ionic yields (observed with di-halobenzenes targets and with benzene itself, displaying a clear non-diatomic behavior where important fragmentation of the benzene ring takes place [6–11]).

Recently, the crossed molecular beam technique has been used for producing negative species in potassium-buckyball collision processes, enabling to show that negative parent C_{60}^- is the only anion formed at energies well below the fragmentation take place [15]. Doubly charged negative ions C_{60}^{2-} (which are metastable in gas phase) are not possible to be formed in these single electron transfer process.

Performing time-of-flight mass spectrometry in a broad dynamical regime where collision induced negative fragmentation takes place, one can selectively induced electronic excitation allowing to study the negative fragmentation of the fullerene anion, which is not possible to observe through simple electron attachment techniques [15–17].

The sensibility of the technique to the internal nuclear rearrangement of the parent negative ion has already been demonstrated for the system K + CH_3NO_2 [9], where assuming an appropriate kinetic model for isomerization of the negative ion, it was possible to estimate that it occurs in about 1 μs, after which fragmentation takes place.

Regarding our target in this work, advances made in the last decade in the methods to produce C_{60} have resulted in the availability of substantial amounts of this cluster [18–20]. The truncated icosahedron shape of buckminsterfullerene is chemically very stable which lays in the Euler's pentagon closure principle and pentagon non-adjacency. Randic et al., using electric circuit theory (conjugated-circuit theory of aromaticity) placed these principles on a firm theoretical basis [21]. The several plausible isomers of C_{60} differ in chemical connectivity and most of them will be obviously chemical reactive with dangling carbon bonds and thus less stable.

Theoretical simulations of C_{60} formation have always produced C_{60} with defects [22], and the smallest possible deviation from the perfect buckyball structure is the so-called "defect" C_{60} [23]. All the atoms in defect C_{60} are still sp^2 bonded. Surprisingly, its binding energy is only 1.6 eV smaller than that perfect C_{60}. However, the transformation between the perfect and the defect structures is separated by a large energy barrier and thus requires high temperatures and long annealing times [23].

For the neutral cluster C_{60}, most isomers can be constructed by sequential rotations of pairs of carbon atoms about their bond center, and such transformation is called "concerted exchange" or Stone-Wales transformation, in analogy to a corresponding process in solids [24]. This should be the lowest energy path, since at most two bonds are broken at any point along the path. In order to locate the saddle point along the concerted path trajectory, ab initio molecular dynamics adiabatic trajectory simulations have been performed [23]. The transition state (highest point along this path) was found and the saddle point energy is 5.4 eV above that of the defect C_{60}. In experiments, high growth temperatures lead to a much increased yield of C_{60}, but the 5.4 eV barrier is still high enough that even at 1000–2000 K a substantial fraction of C_{60} could be trapped in metastable states. However, no isomers other than buckminsterfullerene have been detected to date. Given the low energy of the defect structure and the height of the barrier, some fraction of defect C_{60} should still survive the formation process (which proceeds in cluster formation via third body collisional cooling to remove the heat generated by the fusion of clusters).

In the neutral C_{60} there are 1812 possible conformational isomers and 20 of them have more than the 12 500 Kekulé which were found for the icosahedral C_{60} [25]. From those 20 isomers most are prolate and a few oblate, being three of them approximatively spherical and from those, the isomer with the larger number of Kekulé structures is the prolate with the most far from sphericity shape, which means the isomer with the largest structural strain (introduced in curving the planar system of double bonds into a closed cage) [25]. The reason for the additional stability of the neutral icosahedral C_{60} relies in the fact that it is the only one possessing a Kekulé structure where all the hexagons have three double bonds and all the pentagons have only single bonds. The perfect C_{60} has indeed a huge stability which results from the combination of the π electronic stability with a low mechanical structural strain. It is the only isomer possessing isolated pentagons, and their Kekulé structures do not contribute with equal weight for the energy of the electronic ground state [25].

Density functional theory [26–35] methods have been used to obtain equilibrium geometry configurations of molecules and clusters. Geometry optimisation of C_{60} under I_h symmetry using the hybrid B3LYP density functional approach within Gaussian98, has been performed [44], and a better quality basis set was used for all carbon atoms (6–31G(d)). Because of symmetry constraints, there is only one value for each kind of bond ([6:6] and [6:5]), and [6:6] distances are smaller than the [5:6] ones (Fig. 1A).

The capture of one electron by the C_{60} results in an electronic configuration which implies a Jahn-Teller distortion of the buckyball cage. One can assume that the minimum value for C_{60}^- radius is similar with the van der Waals radius of C_{60}, which is about 0.5 nm [36]. Since the calculated HOMO-LUMO gap in neutral defect C_{60} is 0.6 eV smaller than that of neutral buckminsterfullerene [23], one can assume a similar proportion for the HOMO-LUMO gap in both negative ion isomers.

Anion geometry optimization without any symmetry constraints (unrestricted calculation for the spin unpaired species) leads to changes in the C–C distances [46]: in the anion [6:6] distances are longer while the [6:5] ones remain practically unchanged. Due to the extra electron, symmetry is broken inside the pentagon and one C–C bond is weakened (Fig. 1B). Wiberg indices (reflecting the strength of the bonds) indicates that [6:6] bonds are

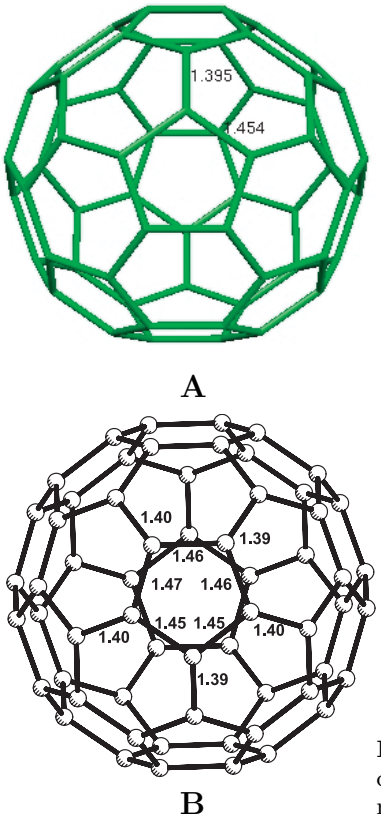

Fig. 1. Structure of C_{60} cluster: (A) neutral; (B) negative ion.

weakened upon ion formation [46]. C_{60} LUMO is mainly π^* [6:6] character. The predictions are that upon ion formation, the extra electron should localize mainly in this orbital producing the weakening of the [6:6] bonds, which can even break. A similar effect has been already confirmed with benzene [12].

Collision induced positive fragmentation can also be used for observation of vibronic effects, and state-of-the-art regarding the target C_{60} has been indicating that mass spectra strongly depends on the time scale which is imposed by the collision energy used. At low energy, one usually induces predominantly vibrational excitation on the fullerene, giving rise to a massive fragmentation; on the other hand, at very high energy ion collisions, electronic excitation is predominantly induced, and the mass spectra are similar to those observed in femtosecond laser excitation or electron impact [37–43].

2 Experimental

A crossed molecular beam set-up configuration with a neutral C_{60} effusive source assembled in the collision chamber, already described elsewhere [15,44], was used in order to produce a C_{60} neutral flux focused in the collision volume. Such C_{60} beam intersects at 90° a fast hyperthermal flux of neutral potassium atoms, formed in a resonant charge exchange source of the Aten type [45]. Such source has an oven connected with a charge exchange chamber, an ionizer tungsten ribbon and two ion extraction electrodes. K^+ ions are produced by surface ionization of the neutral vapor K atoms, and accelerated with an electric field. By resonant charge exchange, the hyperthermal K^+ ions collide with neutral thermal K atoms, producing fast neutral K atoms. Their energy is given in electron-volt by $0.9V_{ion} - 2.4$, where V_{ion} stands for voltage applied to the ionizer. The energy spread of this beam is 0.3 eV and it is collimated by two rectangular slits of 0.2 mm wide. The intensity of the neutral hyperthermal potassium beam is monitored with a surface ionization detector of the Langmuir-Taylor type [14] located in the forward direction prior to the collision volume. The estimated flux in the collision volume is 4.2×10^{12} atoms cm^{-2} s^{-1}.

The fullerene oven is charged with C_{60} powder (99.99% purity from MER Corporation USA) and by heating it up (typical operation temperatures are in the range of 723 up to 888 K) sublimation takes place which gives rise to the production of a C_{60} neutral effusive beam. This beam is captured by a cryogenic pump operating at 18 K and located in front of the oven. Through this cryopumping, random molecular reflection by the chamber internal walls is avoided and so noise in the collision volume is reduced. Due to the high temperatures the C_{60} oven operates, an assembled thermal shielding assures that temperature on its external surface is about three times lower than the internal oven temperature [15].

The highest temperature used in the experiments is 888 K, since according to the oven geometry, above such temperature the molecular flux condition is violated. The C_{60} molecules effuse through a 0.5 mm diameter orifice, which results in an estimated flux of 2.4×10^{15} molecules s^{-1} cm^{-2} at the collision zone.

With such configuration, atomic collisions with buckminsterfullerene involving electron transfer can be performed, and the dynamical study of the ion-pair formation process $K + C_{60} \rightarrow K^+ + C_{60}^-$ is probed in a wide range of collision energy (10 eV up to 500 eV), by using time-of-flight mass spectrometry. A schema of the time-of-flight mass spectrometer is shown in Figure 2. The negative species formed in the interaction region are extracted normal to the plane of the crossed beams by applying a pulsed electric field, 2.0 μs long in a 100 μs duty cycle. Subsequently, they are accelerated into a two drift region time-of-flight mass spectrometer with a total flight path of 27.5 cm. In the first region species were accelerated up to 65 eV and in the second one up to 800 eV. Finally they were accelerated up to 1200 eV and detected with a channeltron electron multiplier.

The interaction volume defined by the intersection of the two beams plays the role of a typical TOF ion source. The actual collision volume geometry is trapezoidal but it can, in a first approximation, be consider a rectangular one, as the difference in the time span will be minimal. Since only single collisions take place in between two pulses, a stationary density of ions n is built up in the source, which is given by the product of the number of anions formed per second and per unit of volume, with the residence time of the ions in the source; this time is equal to the length of the source along the direction of the

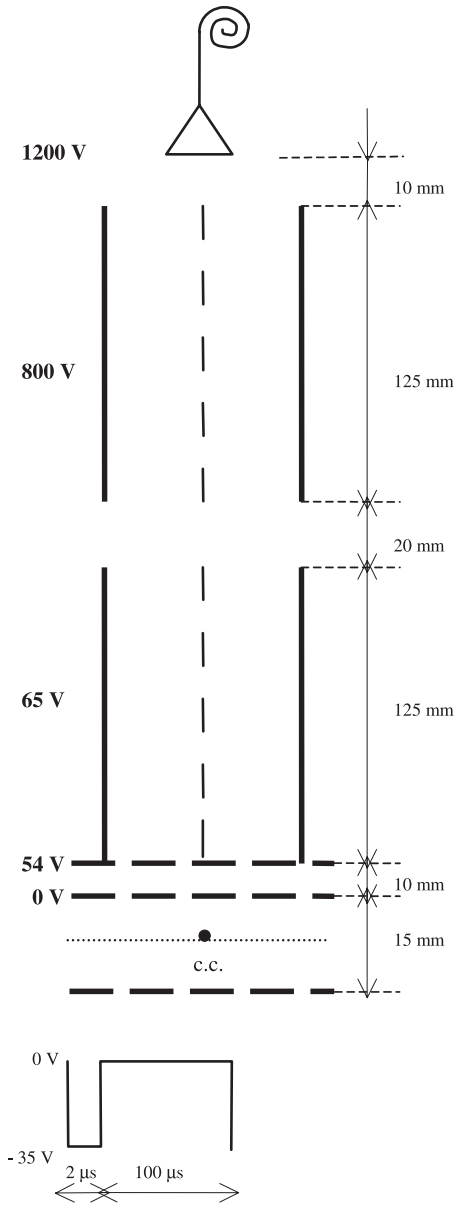

Fig. 2. Time-of-flight configuration.

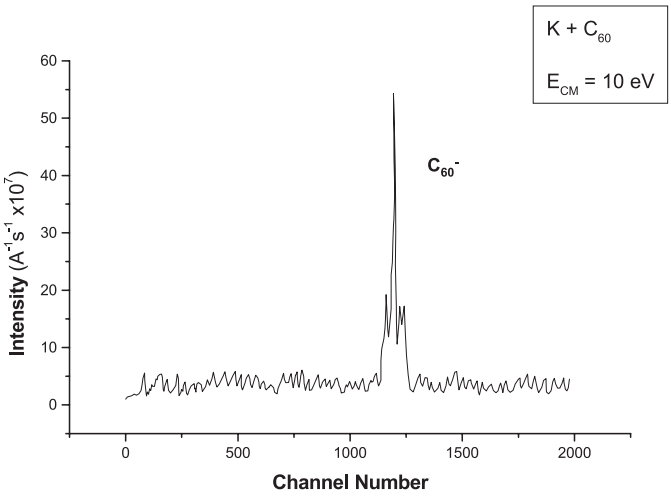

Fig. 3. Time-of-flight mass spectrum obtained at low energy (center of mass collision energy is 10 eV and the C_{60} oven's temperature 843 K). The pulsed extraction voltage is –35 V.

thermal beam (60 mm) divided by the velocity v of the parent fullerene cluster. When the pulse is started, anions are extracted in the direction perpendicular to the plane of the beams with a velocity much larger than v. So the existing ion density is extracted in a time span estimated to be about ten times shorter than the pulse length of 2 μs. Such average density, existing during the remainder of the pulse, is very small with respect to the original one. After the 2 μs pulse, a new building up of ion density is started.

The vacuum during the operation of the two beams was kept at 10^{-4} Pa, assuring a single collision performance.

Data acquisition was carried out on a 2046 channel multichannel analyser working in the Pulsed Height Analysis mode. The TOF spectra were obtained after a selected accumulation time considered enough to provide data with good statistics. The multichannel analyser records each TOF spectrum as function of the channel number N. The conversion factor between the multichannel analyser channel number N and the time-of-flight t (in microseconds) is dictated by the range of the time analyzer (80 μs), being given by:

$$N = 25.6t. \tag{1}$$

The intensity for each peak in the spectrum is given by its area which is the invariant quantity with respect to the mass m [12]. The full width half maximum (FWHM) of the parent ion peak displayed in the TOF spectra is proportional to $m^{1/2}$, and the main contribution to the FWHM of the peak comes from the acceleration region [12].

A previous calibration of the TOF spectrometer was done by performing several collisions of neutral potassium atoms with different precursors of the target beam (including CH_3I, CCl_4 and $FeBr_2$) and the result is a best fitted calibration curve for the mass m (in Dalton) given by the following expression:

$$m = 4.769 + 0.053N + 4.222 \times 10^{-4}N^2. \tag{2}$$

Collisions of neutral potassium atoms with C_{60} molecules are performed at several energies ranging from 10 eV up to 500 eV, keeping constant the values of the electrostatic potentials in the TOF, accordingly to those displayed in Figure 2 [44,46]. Each time-of-flight mass spectrum is recorded at a chosen collision energy within that range.

3 Results

In the collision of potassium atoms with C_{60}, performed at low energy (10 eV) the time-of-flight mass spectrum shows a well defined contribution at about $N = 1241$ (Fig. 3)

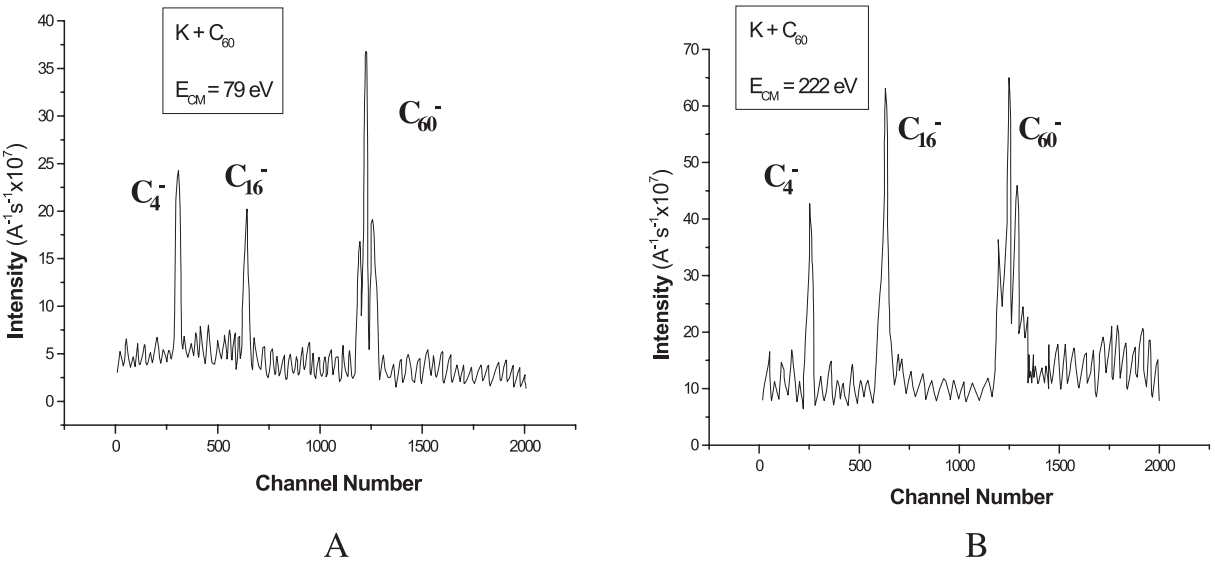

Fig. 4. Time-of-flight mass spectrum obtained at high energies (center of mass collision energies are 79 eV (A) and 222 eV (B); C_{60} oven's temperature is 843 K). The pulsed extraction voltage is –35 V.

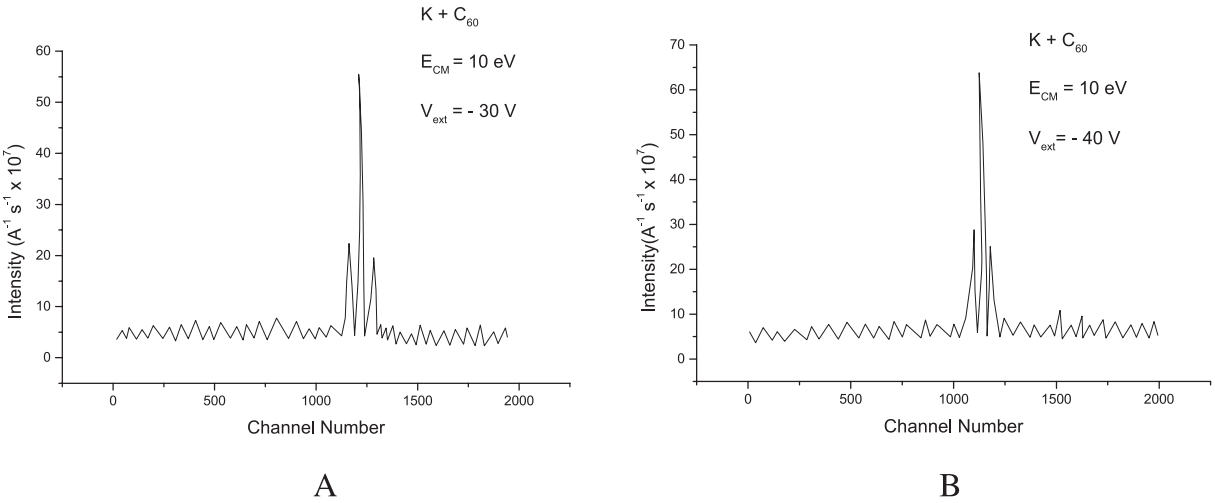

Fig. 5. TOF spectra recorded at a fixed collision energy (10 eV) and two different pulsed voltages: –30 V (A), and –40 V (B). C_{60} oven's temperature is 843 K.

which accordingly to expressions (1) and (2) can be assigned to the anion C_{60}^- ($60 \times 12 = 720$ Dalton).

The reason for not using in addition collision energies below 10 eV lies on the experimental limitation of our charge exchange source, which does not give enough intensities in order to achieve good signal-to-noise ratios in the accumulation TOF spectra.

Time-of-flight mass spectra were obtained for several higher collisions energies and Figure 4 shows the corresponding ones at 79 eV and 222 eV. All the spectra intensities are normalized to the primary alkali beam intensity which is monitored with the Langmuir-Taylor detector, and so they are displayed in inverse units of electric current per second.

In the K + C_{60} collision all the spectra show evidence of parent negative ion formation. At low energies only this contribution comes out (Fig. 3); however increasing the collision energy additional fragmentation is observed (Fig. 4) and contributions from the anions C_4^- and C_{16}^- become evident (making use of the calibration curve (2) mentioned above). Nevertheless, the contribution from the parent C_{60}^- is always present in all spectra taken in our experimental collision energy range.

The above mentioned TOF spectra were all obtained for an extraction pulsed voltage of –35 Volts, but some additional TOF spectra have been recorded at a fixed collision energy (10 eV) and different pulsed voltages (–30 V and –40 V, as shown in Fig. 5). The choice for the close proximity in these pulsed voltage values was made in order to avoid the need for correcting the other voltages of the TOF grids due to ion re-focusing reasons.

The total and partial cross-sections corresponding to negative ion formation for the buckminsterfullerene are respectively displayed in Figures 6 and 7. Since the density

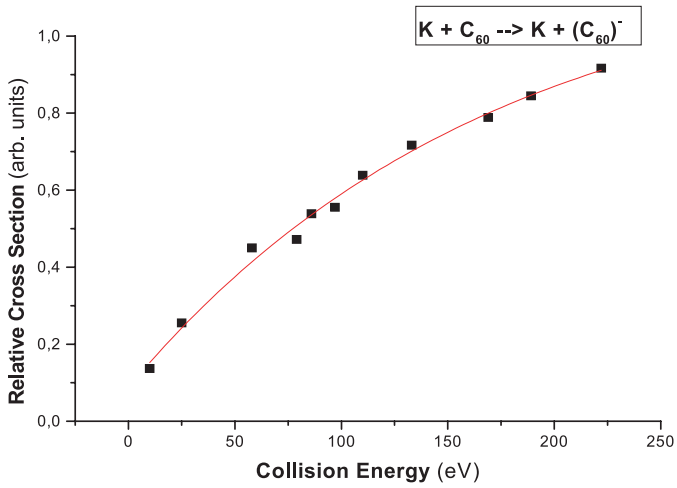

Fig. 6. Total relative negative ion cross-section in K + C_{60} collision.

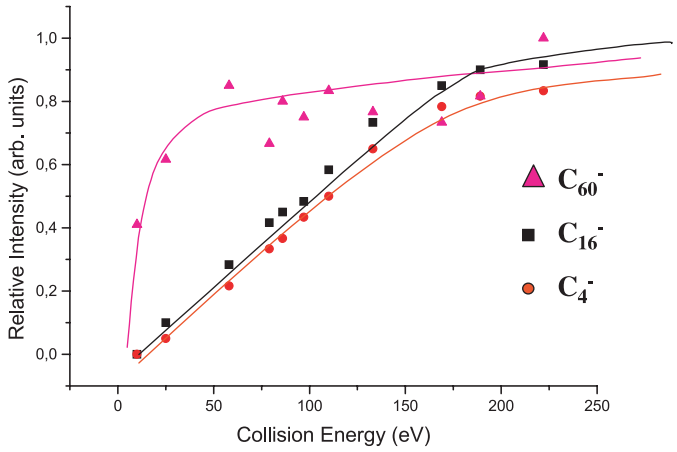

Fig. 7. Partial negative ion cross-sections in K + C_{60} collision.

of the target molecular beam in the collision region is not monitored, such cross-sections do not correspond to absolute values, although the intensity of the target beam is assumed to not significantly vary (as the oven temperature is kept constant). In Figure 7 the relative intensities were taken from the estimated area under each TOF peak. This method has an error of about 5%, and can explain certain apparent inconsistencies between the values shown in Figure 4 and the cross-sections of Figure 7.

4 Discussion on electron harpooning and anion fragmentation

The time-of-flight spectra recorded in our broad dynamical regime where collisional electron transfer takes place, show evidence of negative ion formation, being the ratio of intensities between the parent ion and fragment ions clearly dependent on the collision energy. The induced negative fragmentation is assumed to proceed via the prior formation of the excited parent ion C_{60}^-, and this induced vibronic excitation should be very selective since it results from non-adiabatic effects, accordingly to the harpooning mechanism [1–13]. Actually, taking into account the high number of internal degrees of freedom and the wide collision energy range involved in these experiment, the collision induced fragmentation exhibits an unexpected high selectivity. This fact is mirrored in the very small number of anion fragments observed (C_4^- and C_{16}^-) even at the highest collision energy measured. This strongly contrasts with several other methods of studying the ionic fullerene cage breaking apart (positive or negative), as for instance photofragmentation, electron impact, positive ion-C_{60} collisions, where it has been observed a predominantly induced massive fragmentation [37–43]. The C_{60}^- ions formed above 7 eV in electron attachment studies [39] are seen to thermally detach, but if the imparted energy can be quickly removed before thermal detachment can occur, then C_{60}^- ions will be very stable. This is likely to explained why our C_{60}^- continuously rising cross-section at high energy does not display any trend to go down.

Further comparisons with free electron attachment results are useless in the aim of this work, since as it was explained in the introduction, such technique is unable to produce negative fragmentation and significant vibronic excitation of the fullerene cluster, as well.

From the electron harpooning model involving the crossing of ionic and covalent diabatic potential surfaces [1–8], it is roughly possible to infer about the K–C_{60} distance r_c, at which the electronic transition would take place. In fact, since the interaction potential of the neutral system is weak and the ionic attraction potential is due to the sum of the Coulombic attraction term $\sim r^{-1}$ with an induction potential function due to polarization $\sim r^{-4}$, then a lower limit for the crossing distance (in angstrom) can be obtained (if it occurs far enough from the repulsive regions of the two potential surfaces), by the following identity:

$$I - EA = 14.42 \left[1 + \alpha / \left(2r_c^3\right)\right] / r_c \qquad (3)$$

where I is the well-known ionization potential (in eV) of the electron donor potassium atom (4.33 eV) and α the polarizability of C_{60}^- in angstrom^3. The perfect buckyball has a mean diameter of about 0.7 nm (its cavity almost reaches 0.4 nm in diameter, and the ball outer diameter is about 1 nm) [49] and its electron affinity EA is about 2.65 eV [40,56]. The high polarizability and effective number of valence electrons in C_{60} are 86 angstrom^3 and 240 respectively, and C_{60} does not change significantly its polarizability upon ionization [57]. Therefore, the estimated result applying (3) is $r_c = 0.9$ nm, which means that the electron transition occurs at a distance very close to the buckyball radius, where the repulsive forces cannot be neglected, and so these estimations should be taken with severe limitations.

Parent ion reveals itself as a very stable anion in the experimental collision energy range, and taking into account our observed fragmentation patterns, it can be inferred that C_2 sequence loss mechanism which has been explaining other types of fullerene collisional experiments [49], does not seem to be relevant in our case. In fact, the

electron transfer induced negative fragmentation process is very selective and as above mentioned, it is substantially different from the mechanisms proposed by other authors to explain positive fragmentation and photofragmentation patterns [37–43].

Regarding the negative total cross-sections, there is a substantially different behavior in buckminsterfullerene when compared with those of some aromatic and non-aromatic targets previously studied, using the same type of projectile atom (potassium in this case) [2,3]. As it can be seen in Figure 7, the cross-section is continuously increasing, even at very high energies. In turn, ion-pair formation total cross-sections of benzene and other poly-atomic aromatic targets that have been measured [12] present a Landau-Zener maximum at a collision energy of about 100 eV, which is a quite high energy value when compared with the same maxima obtained for other non-aromatic electrophilic molecules [8]. Such behavior has been explained by the possibility that the reactive channel can be very important over a wide range of collision energies [8], as it was suggested to occur with the halogen abstraction reactive channel in collisions of Cs + UF_6 [47] and K + C_6F_6 [48]. The absence of the maximum for the case of C_{60} is likely due to the possibility that the reactive channel K + $C_{60} \rightarrow KC_n$+C_{60-n} is not playing a so important role as the ionization process does, even at collision energies just above the ion-pair formation threshold.

Concerning the relative cross-sections for the production of negative ions, one can say that selective fragmentation in the fullerene is operating in a different way of what has been previously observed with benzene [12]. In fact, in our electron transfer experiments the negative fragmentation of the C_{60} has revealed a *non-diatomic* type behavior as well as benzene, but contrarily to what is happening with this C_6H_6 molecule (where the parent ion was not detected), in the fullerene the parent ion is very stable and still formed even at collision energies well above the ion-pair formation threshold. Probably, the selective negative fragmentation pathways taking place in both targets follow some criteria dictated by the higher stability of the $C_2H_x^-$ fragments (detected in benzene) compared with C_2^-. Actually, fullerene is not a benzene-like molecule in 3 dimensions, where one hydrogen atom is attached to each one of the carbon atoms.

In a simple quantum-chemical description of the electronic structure of C_{60} based on the molecular orbital approach, each carbon atom contributes with 4 valence orbitals ($2s$, $2p_x$, $2p_y$ and $2p_z$) and thus C_{60} has 120 occupied molecular orbitals and 120 unoccupied or virtual MO's. With some approximations (C60 is not planar) 60 MO's (30 occupied and 30 virtual) can be considered of π type and the remaining 180 orbitals of σ type. In analogy with large aromatic compounds, the highest occupied MOs (HOMOs) and the lowest unoccupied MOs (LUMOs), which determine the lower electronically excited states are of σ type.The electronic ground state of C_{60} is a closed shell. The lowest electronic absorption of C_{60}^- is theoretically expected to occur at about 0.6 eV, where the electron in the T_{1u} ground state orbital makes a transition to the T_{1g} orbital [51].

The possibility of ring fragmentation by the simultaneous breaking of two C–C bonds, one via the occupation of LUMO, and the other via second LUMO is very unlikely since it will need a high energy supply (at least 6 eV). It is more likely that one bond is broken, followed by a rearrangement leading the second bond to break apart. This could explain the delay of about 1.5 μs, observed in the TOF spectrum for the two fullerene negative fragments (C_4^- and C_{16}^-), relatively to their expected flight times (Fig. 4). The expected flight times are easily estimated making use of expressions (1) and (2). Such value for the delay is of the same order of magnitude of other delays already found for some other negative fragments of di-halobenzenes, which seem to follow a two-step fragmentation mechanism [10,11]. Such two-step fragmentation mechanism is likely to be facilitated by the rotating-pair of carbon atoms in the defect C_{60} transition, already mentioned in the introduction to this work.

5 Discussion on fullerene anion metastable conformers

In addition and quite surprisingly, two satellite contributions have been observed in the band structure of C_{60}^- parent ion TOF spectrum (located on both sides of the main central peak), as it is clearly displayed in Figures 3, 4 and 5, for all the spectra taken at the several collision energies. This effect in the spectra was only observed for the parent ion contribution and it is not present for the two ionic fragments. The time shift corresponding to the observed satellite peaks in the C_{60}^- TOF spectra is of the order of 1–3 μs, relatively to the central main peak.

Accordingly to the common available Tables of Isotopic Masses and Natural Abundances the carbon isotopes ^{12}C and ^{13}C represents respectively, about 98.9% and 1.1% of the total number of natural carbon atoms in C_{60}. Therefore this distribution of isotopic masses is completely unable to explain the two observed satellite peaks in the TOF spectra. Moreover, the corresponding mass shifts with respect to the central C_{60}^- peak, observed in the TOF spectra, are much smaller than 12 Dalton (the carbon atomic mass), and then one cannot explain the two small peaks by eventual abstraction or addition of a carbon atom to the negative buckyball cage.

These facts seem to point the formation of distinct conformational metastable C_{60}^- isomers (prolate and oblate), which can be formed in the diabatic negative potential surface. Since the calculated HOMO-LUMO gap in neutral defect C_{60} is 0.6 eV smaller than that of neutral buckminsterfullerene [23], one can assume a similar proportion for the HOMO-LUMO gap in both negative ion isomers.

This presumed detection of different spheroidal metastable C_{60}^- conformers (Fig. 8) was made possible due to an electric effect operating at the nanoscale. Actually, for a negative spheroidal conductor (note that the additional electron in the cage is completely delocalized) immersed in an uniform extraction electric field, its need to

Fig. 8. C_{60}^- spheroidal shapes.

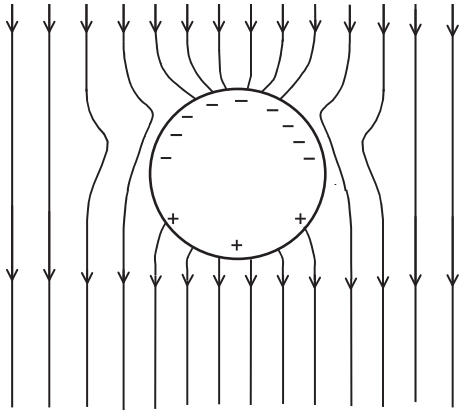

Fig. 9. Negative charged sphere in an applied uniform electric field.

keep a zero electric field inside, imposes an asymmetric surface charge distribution, which in the neighbourhood of the fullerene cage distorces the applied surrounding uniform electric field, and gives rise to an electric field gradient along the linear dimension of the C_{60}^- macromolecular cage, in the direction of the applied field (see Fig. 9). Actually, such field gradient is not negligeable compared with the fullerene diameter. Since the field gradient is dependent on the shape assumed by the fullerene cage, the extraction force applied to the negative ion will be different for each possible negative conformer (prolate, oblate and sphere).

The calculated difference in time-of- flight, between the fullerene anion spherical mass and each one of the other two spheroidal isomers is of the same order of magnitude as the one experimentally observed (1–3 μs). The calculations are presented in the Appendix A of this article. They are inspired in simple classical electrodynamic estimations of the C_{60}^- time-of-flight (based on the TOF mass spectrometer electric potentials and lengths displayed in Fig. 2) and in the surface charge density σ of a conducting ellipsoid [57]. Such calculations have been performed making use of the *Mathematica* 5.1 program [52,53].

The formation of such conformational isomers is likely to be induced by the strong polarization of the C_{60}^- in the presence of the K^+ projectile ion, during the collision lifetime.

When the positive charge of the K^+ ion is close interacting with the highly polarizable fullerene anion, an electric dipole is induced, and this polarization effect is likely to induce the stabilization of some anion spheroidal conformers. These metastable negative states together with the ground negative state (sphere) should be adiabatically coupled at large distances.

In addition, the previously mentioned high selectivity observed in the C_{60}^- fragmentation is also likely to be favoured by such internal rearrangement pathway in the potential energy surface.

The three observed conformational isomers should correspond to the most stable states resulting from the multiple carbon atoms interactions. The spherical conformer has a zero quadrupole electric moment and is the most stable. When we are considering the oblate and prolate conformations, we are most likely assuming an average among all the possible isomers (which in the neutral C_{60} are known to be 20, as it was explained in the introduction of this work).

Our calculations (see Appendix A), the oblate shape takes more time than the spherical perfect C_{60}^- to travel through the flight path, and in turn the prolate shape will be the first of the three to be detected. Therefore, accordingly to our model, the satellite contribution appearing at the largest time-of-flight in the spectra should correspond to the oblate isomer of C_{60}^- and the satellite peak appearing earlier can be assigned to the corresponding prolate isomer.

Also accordingly to the calculations (see Tab. 1 in Appendix A), as stronger is the applied extraction field more earlier the prolate reaches the detector and in turn the oblate isomer will arrive with an even larger delay. This is in clear agreement with the experimental variation of the satellite time shifts with the extraction field magnitude. Actually, as it can be confirmed from Figures 3 and 5, as larger is the applied electric field more larger are such time shifts. Moreover, the estimated time shifts variations agree, in first approximation, with the experimental ones (see Appendix A).

At low collision energies the relative areas of the two satellite contributions in the TOF spectra are quite similar but as far as more energy is put in the collision, the contribution at the higher time-of-flight seems to become more relevant. This could indicate that as more internal energy is deposited in the parent ion by the collision more likely is the formation of the oblate isomers contribution and so, in the negative ion, the oblate metastable state should correspond to a higher energy than the prolate state. Note that (see Introduction of this paper) in the neutral C_{60} cluster the prolate shape isomers are in a larger number than the oblate ones.

The fact that the two satellite peaks for the C_{60}^- contribution are present in the TOF spectra even at the largest measured collision energy (300 eV) is a clear indication that their relevance do not significantly depend on the collision time.

6 Final concluding remarks

Our technique of ion-pair formation in K + C_{60} collisions has been successful in the detection of the buckyball metastable negative conformers and also its negative

fragments due to the broad dynamical regime in use (10–500 eV), which allows to deposit a variable amount of internal energy in the C_{60}^- anion. This was not made possible by other close related techniques, as for instance in the case of near-grazing surface scattering of neutral C_{60} with surface targets [50], where the energies involved are lower by several orders of magnitude. In addition, performing Penning ionization collisions of thermal C_{60} with supersonic metastable rare-gas atoms Rg, it is possible to detect C_{60}^+ ions and electrons, and explain the results assuming an intermediate ionic state Rg^+–C_{60}^- [54], which influences the energy distributions measurements of the ejected electrons. However, with such technique the collision energies are very small and then it was not possible to gain indirect information on metastable negative states of C_{60}.

This work has been developed under support from FCT/MCTES in particular through the project POCTI/FIS/43627/2000.

Appendix A: Estimation of the C_{60}^- conformers flight times

A.1 Surface charge density for a conducting spheroidal body

An ellipsoidal surface can be expressed in Cartesian coordinates by [52,53]:

$$\frac{x^2}{a^2}+\frac{y^2}{b^2}+\frac{z^2}{c^2}=1 \tag{A.1}$$

and the surface charge density σ on a conducting ellipsoid can be written [57]:

$$\sigma=\frac{q}{4\pi abc\sqrt{\dfrac{x^2}{a^4}+\dfrac{y^2}{b^4}+\dfrac{z^2}{c^4}}} \tag{A.2}$$

which in the case of a spheroidal surface takes the simplified form [57]:

$$\sigma=\frac{q}{4\pi abc\sqrt{\dfrac{x^2+y^2}{a^4}+\dfrac{z^2}{c^4}}} \tag{A.3}$$

where a, b and c are the lengths of the three ellipsoid axis (with $a=b$) and q is the total charge, which in the case of the fullerene negative ion will assume the electron charge value: $q=-e=-1.6\times10^{-19}$ Coulomb. In the case of an oblate shape we have $a>c$ and in the prolate $a<c$.

A.2 Calculation of a spheroidal elementary surface

In the case of a spheroidal surface of revolution (oblate or prolate), obtained by the rotation of a line $r=r(z)$ around the zz-axis, the expression for r is the following [52,53]:

$$r(z)=a\sqrt{1-\left(\frac{z}{c}\right)^2} \tag{A.4}$$

and the corresponding elementary surface dS is given by [52,53]:

$$dS=2\pi r\sqrt{1+\left(\frac{dr}{dz}\right)^2}\,dz. \tag{A.5}$$

From (4) and (5) it is then possible to find the expression for the spheroidal elementary surface:

$$dS=2\pi a\sqrt{1+\frac{(a-c)(a+c)z^2}{c^4}}dz. \tag{A.6}$$

A.3 Electrostatic force applied on the fullerene anion

By replacing dS and the surface charge density σ in the expression of the elementary force:

$$dF=dqE=\sigma dSE \tag{A.7}$$

(where E represents the total electrostatic field) one can obtain three expressions for the three components of the force relatively to each of the spatial coordinates:

$$dF_x=\frac{q^2x}{4\pi a^3c^4\varepsilon_0}\left(\frac{c^2-z^2}{a^2c^2}+\frac{z^2}{c^4}\right)^{(-3/2)}\times\sqrt{1+\frac{(a-c)(a+c)z^2}{c^4}} \tag{A.8}$$

$$dF_y=\frac{q^2y}{4\pi a^3c^4\varepsilon_0}\left(\frac{c^2-z^2}{a^2c^2}+\frac{z^2}{c^4}\right)^{(-3/2)}\times\sqrt{1+\frac{(a-c)(a+c)z^2}{c^4}} \tag{A.9}$$

$$dF_z=\sqrt{1+\frac{(a-c)(a+c)z^2}{c^4}}\times\left[\frac{q^2z}{4\pi a^3c^4\varepsilon_0}\left(\frac{c^2-z^2}{a^2c^2}+\frac{z^2}{c^4}\right)^{(-3/2)}+\frac{qE_{ap}}{2ac}\left(\frac{c^2-z^2}{a^2c^2}+\frac{z^2}{c^4}\right)^{(-1/2)}\right] \tag{A.10}$$

where E_{ap} is the applied uniform electric field (given experimentally by the ratio between the extraction pulse voltage and the distance between the parallel extraction electrodes), which is equal to $(E-\sigma/\varepsilon_0)$, being ε_0 the vacuum electric permitivity.

In our simulations we have ignored the components of the force relatively to the x and y coordinates, because they would not produce any effect on the time-of-flight of the ion.

In first approximation, if one considers that negative electric charge only distributed on the upper half part of the spheroidal isomer, the component z of the force will be computed by the integral of dF_z, for z between $-c$ and c. The component z of the force will then assume a different value for each one of the three isomers.

Table 1. Estimated and experimental C_{60}^- time-of-flight differences with respect to the spheroidal conformer at different extraction voltages. Since the prolate conformer appears at the lowest time-of-flights, their time shifts are reported as negative in opposition with the oblate delays which are considered positive.

	−30 V			−35 V			−40 V		
	TOF (μs)	Δt_{teo} (μs)	Δt_{exp} (μs)	*TOF* (μs)	Δt_{teo} (μs)	Δt_{exp} (μs)	*TOF* (μs)	Δt_{teo} (μs)	Δt_{exp} (μs)
oblate	50.0	+3.7	+2.6	46.3	+3.4	+2.5	43.4	+3.2	+2.2
prolate	43.5	−2.8	−1.6	40.3	−2.6	−1.5	37.8	−2.4	−1.3
sphere	46.3	—	—	42.9	—	—	40.2	—	—

A.4 Simulation of the time-of-flight

Taking into account the geometrical configuration of the TOF mass spectrometer (Fig. 2), the total time-of-flight t for the anion is estimated by application of classical equations of motion, applied to each one of the six identified path lengths (in Fig. 2), considering the two drift and the four acceleration regions, where t_j and t_i stands for such corresponding times:

$$t = \sum_{i=1}^{4} t_i + \sum_{j=1}^{2} t_j$$

$$\text{with} \quad t_i = m\frac{v_0^i + \sqrt{-v_0^{i^2} + \frac{2F_i}{m}(x_i - x_{0_i})}}{F_i}$$

$$\text{and} \quad t_j = \frac{x_j - x_{0j}}{v_0^j} \qquad \text{(A.11)}$$

where m is the ion mass, F_i is the computed electric force in each acceleration region of the spectrometer, $v_0^{i,j}$ are the initial velocities in each step region of the mass spectrometer and $(x_{i,j} - x_{0i,j})$are their respective lengths.

Table 1 summarizes the ion time-of-flights obtained with our estimations, for each conformational isomer at the three experimental extraction potentials.

References

1. D.R. Herschbach, Adv. Chem. Phys. **10**, 319 (1966)
2. A. Baede, J. Los, Physica **52**, 422 (1971)
3. P.K. Parks, A. Wagner, S. Wexler, J. Chem. Phys. **56**, 5502 (1973)
4. E.W. Rothe, S.Y. Tang, G.P. Reck, Chem. Phys. Lett. **26**, 434 (1974)
5. R.N. Compton, P.W. Reinhardt, L.D. Cooper, J. Chem. Phys. **68**, 4360 (1978)
6. P.R. Brooks, Science **193**, 11 (1976)
7. K. Lacmann, Adv. Chem. Phys. **42**, 513 (1980)
8. A.W. Klein, J. Los, E.A. Gislason, Phys. Rep. **90**, 1 (1982)
9. R.F.M. Lobo, A.M.C. Moutinho, K. Lacmann, J. Los, J. Chem. Phys. **95**, 4360 (1991)
10. R.F.M. Lobo, A.M.C. Moutinho, J. Los, Chem. Phys. **179**, 179 (1994)
11. R.F.M. Lobo, A.M.C. Moutinho, M.J. Calhorda, Chem. Phys. **234**, 265 (1998)
12. R.F.M. Lobo, P.L. Vieira, S.S.M.C. Godinho, M.J. Calhorda, J. Chem. Phys **116**, 9712 (2002)
13. B. Jia, J. Laib, R.F.M. Lobo, P.R. Brooks, J. Am. Chem. Soc. **124**, 13896 (2002)
14. G. Scoles, *Atomic and Molecular Beam Methods* (Oxford University Press, New York, 1988/1992), Vols. 1/2
15. R.F.M. Lobo, N.T. Silva, Rev. Scient. Instrum. **72**, 3505 (2001)
16. O. Elhamidi, J. Pommier, R. Abouaf, J. Phys. B: At. Mol. Opt. Phys. **30**, 4633 (1997)
17. L.G. Christophorou, D.L. McCorkle, A.A. Christodoulides, *Electron-Molecule Interactions and Their Applications*, edited by L.G. Christophorou (Academic, New York, 1984), Vol. 1
18. H.W. Kroto, J.R. Heath, S.C. O'Brian, R.F. Curl, R.E. Smalley, Nature **318**, 162 (1985)
19. W. Krätchmer, L.D. Lamb, K. Fostiropoulos, D.R. Huffman, Nature **347**, 354 (1990)
20. R.E. Haufler, Y. Chai, L.P.F. Chibante, S. Maruyama, R.E. Smalley, *Clusters and Cluster Assembled Materials*, edited by R.S. Averback, J. Bernholc, D.L Nelson, MRS Proc. **206**, 627 (1991)
21. M. Randic, Chem. Phys. Lett. **38**, 68 (1976)
22. J. Chelikowsky, Phys. Rev. Lett. **67**, 2970 (1991)
23. J. Yi, J. Bernholc, J. Chem. Phys. **96**, 8634 (1992)
24. K.C. Pandey, Phys. Rev. Lett. **57**, 2287 (1986)
25. S.J. Austin, P.W. Fowler, P. Hansen, D.E. Manolopoulos, M. Zheng, Chem. Phys. Lett. **228**, 478 (1994)
26. R.G. Parr, W. Yang, *Density Functional Theory of Atoms and Molecules* (Oxford University Press, Oxford, 1990)
27. T. Ziegler, Chem. Rev. **91**, 651 (1991)
28. P. Pyykko, Chem. Rev. **97**, 597 (1997)
29. M.J. Frisch et al., *GAUSSIAN 98*, Revision A8, Gaussian, Inc., Pittsburgh, PA, 1998
30. A.D. Becke, J. Chem. Phys. **98**, 5648 (1993)
31. C. Lee, W. Yang, R.G. Parr, Phys. Rev. B **37**, 785 (1988)
32. C. Moller, M.S. Plesset, Phys. Rev. **46**, 618 (1934)
33. M.J. Frisch, M. Head-Gordon, J.A. Pople, Chem. Phys. Lett. **166**, 275 (1990)
34. J. Cioslowski, B.B. Stefanov, Mol. Phys. **84**, 707 (1995)
35. R.F.W. Bader, *Atoms in Molecules: A Quantum Theory* (Oxford University Press, Oxford, 1990)
36. J. Huang, H.S. Carman, R.N. Compton, J. Phys. Chem. **99**, 1719 (1995)
37. L.S. Wang, C. Jin, R.E. Smalley, Chem. Phys. Lett. **182**, 5 (1991)
38. E. Foltin, T.D. Märk, J. Chem. Phys. **98**, 9624 (1993)
39. T.D. Märk, I. Illenberger, J. Chem. Phys. **102**, 2516 (1995)
40. H. Lorents, M. Mathur, Phys. Rev. A **52**, 3847 (1995)
41. H. McHale, J. Mass Spect. **30**, 33 (1995)
42. H. Ehlich, E. Campbell, J. Chem. Phys. **104**, 1900 (1996)
43. F. Will, A. Vandenbosch, UW NPL. Annual Rep **67**, 199 (2000)

44. R.F.M. Lobo, N.T. Silva, M.J. Calhorda, M.S. Costa, P.J. Costa, *Proceedings XX International Symposium on Molecular Beams*, Lisbon (UNL, 2003), pp. 1, 137
45. J.A. Aten, J. Los, J. Phys. E. Sci. Inst. **8**, 408 (1973)
46. R.F.M. Lobo, N.T. Silva, M.S. Costa, *Proceedings XXI International Symposium on Molecular Beams*, Hersonisos (FORTH, 2005), p. 79
47. B.K. Annis, S. Datz, J. Chem. Phys. **69**, 2553 (1978)
48. R.N. Compton, P.W. Reinhardt, Chem. Phys. Lett. **91**, 268 (1982)
49. W.E. Billups, M.A. Ciufolini, *Buckminsterfullerenes* (VCH Publishers, New York, 1993)
50. A. Bekkerman, B. Tsipinyuk, S. Verkhoturov, E. Kolodney, J. Chem. Phys. **109**, 8652 (1998)
51. B. Friedman, Phys. Rev. B. **48**, 2743 (1992)
52. R.J. Gaylord, S.N. Kamin, P.R. Wellin, *Introduction to Programming with Mathematica* (Springer-Verlag, New York, 1993)
53. M.L. Abell, J.P. Braselton, *Differential Equations with Mathematica*, 2nd edn. (Academic Press, Boston, 1996)
54. B. Brunetti, P. Candori, R. Ferramosche, S. Falcinelli, F. Vecchiocattivi, A. Sassara, M. Chergui, Chem. Phys. Lett. **294**, 584 (1998)
55. C. Brink, L.H. Andersen, P. Hvelplund, D. Mathur, J.D. Voldstad, Chem. Phys. Lett. **233**, 52 (1995)
56. H. Yasumatsu, T. Kondow, H. Kitagawa, K. Tabayashi, K. Shobatake, J. Chem. Phys. **104**, 899 (1996)
57. L.D. Landau, E.M. Lifshitz, *Electrodynamics of Continuous Media* (Pergamon Press, New York, 1960)